Technical University of Denmark

DTU

Revisiting Veerman's interpolation method

Christiansen, Peter; Bay, Niels Oluf

DTU Library
Technical Information Center of Denmark

Revisiting Veerman's interpolation method

Peter Christiansen[1] and Niels Bay[1]

Abstract

This paper describes an investigation of Veerman's interpolation method and its applicability for determining sheet metal formability. The theoretical foundation is established and its mathematical assumptions are clarified. An exact Lagrangian interpolation scheme is also established for comparison. Bulge testing and tensile testing of aluminium sheets containing electro-chemically etched circle grids are performed in order to experimentally determine the forming limit of the sheet material. The forming limit is determined using a) Veerman's interpolation method, b) exact Lagrangian interpolation and c) FE-simulations. A comparison of the determined forming limits yields insignificant differences in the limit strain obtained with Veerman's method or exact Lagrangian interpolation for the two sheet metal forming processes investigated. The agreement with the FE-simulations is reasonable.

Keywords

Forming limit curve, Veerman's interpolation method, bulge testing, grid analysis

[1]Department of Mechanical Engineering, Technical University of Denmark, Kgs. Lyngby, Denmark

Corresponding author:

Peter Christiansen, Department of Mechanical Engineering, Produktionstorvet Bygn. 425, 2800 Kgs. Lyngby, Denmark

Email: petc@mek.dtu.dk

Introduction

Sheet metal forming is applied for the production of a large variety of everyday products. Examples are deep drawing of food and beverage cans, stamping of car body panels and stretch forming of car hoods. To ensure sound production with no fracture the material formability is often determined in form of an experimental forming limit diagram (FLD) with the in-plane major and minor strains $(\varepsilon_{min}, \varepsilon_{max})$ on the abscissae and ordinate axis respectively. Such diagrams were first proposed by Keeler[1] for stretch forming and by Goodwin[2] for drawing of sheets determining the local strains by measuring deformation of electro-chemically etched circle grids in sheet stamping production. The forming limits were, however, difficult to estimate with accuracy in stamping production, especially when fracture had occurred leading to excessive

deformation of the circle through which it occurred.

Takashina et al.[3] suggested to measure the strains in three circles, where the middle one contained the fracture, averaging the strains to obtain the limit strain.

By measuring and plotting strains from several circles in the neighbourhood of fracture a more proper definition of the forming limit can be made. These deformed circles (often of elliptical shape) must include ones that are not affected by necking and ones that are. The forming limit curve can then be drawn to fall above those circles that are not-necked and below those that are. Hecker[4] utilized this method on fractured, necked and defect free deformed circles at or close to the fracture in order to determine the FLD.

D'Haeyer et al.[5] suggested a two-step approach for determining instability.

First the blank, containing an electro-chemically etched grid, is deformed to a stage close to necking and strains are measured. Thereafter the blank is deformed a small amount more and strains are measured again. Areas that are necking will increase significantly in strain whereas other areas will only show a minor increase in strain. This method however may require a large number of tests before having determined when necking occurred.

Veerman[6] has pointed out that after the onset of local necking the material outside the neck will not be strained any further and deformation will concentrate inside the neck. It should therefore be possible to detect the onset of localized necking by plotting strain in the necking region versus strain in the region next to necking but not affected by it. Such a curve is sketched in Figure 1. Initially the two areas will deform rather identically and the curve is represented by a straight line inclined 45° to the axes. Then as necking occurs strain concentrate in one area and cease in other areas. Thus the curve will bend towards parallelism with one of the axes.
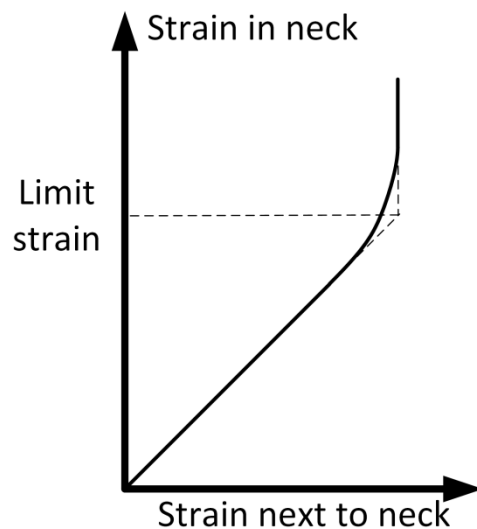

Figure 1. Definition of the limit strain using Veerman's graphical method.

Measurements using optical cameras and subsequent strain determination were performed by Volk et al.[7] who determined the onset of necking as the point where two lines approximating the measured strain at steady growth and after instability intersects one another.

In case of no visible access to the necking area due to contacting punch or die in a production environment another method developed by Veerman[8] may be applied. Based on the assumption that the strain in the neck at the onset of localized necking can be inferred from the strain gradients adjacent to the fracture Veerman[8] has proposed a Lagrangian interpolation formula for the maximum strain ε_{max} based on the strain at three positions on each side of the fracture, see Figure 2. The minimum strain is determined by measuring the deformed circle including or closest to the fracture.

It is the aim and scope of this paper to examine Veerman's interpolation method and its mathematical basis comparing experimental measurements on bulge tests and tensile tests of aluminium blanks with FE predictions of the FLD.

The theoretical basis for Veerman's interpolating method

The basis for Veerman's interpolation method will be derived in order to understand the mathematical foundation and approximations. The derivation is based on Figure 2, which schematically illustrates a deformed circle grid and associated strain distribution around a crack going through one of the circles deformed to an ellipse. The ellipses have centers at positions $(x_0, x_1, x_2, x_3, x_4, x_5)$. The centers of the ellipses are separated by the distances $(\Delta x_1, \Delta x_2, \Delta x_5, \Delta x_6)$ and the two ellipses closest to the fracture have distances Δx_3 and Δx_4 to the crack. The major in-plane strain ε_{max} is calculated for each non-fractured ellipse by
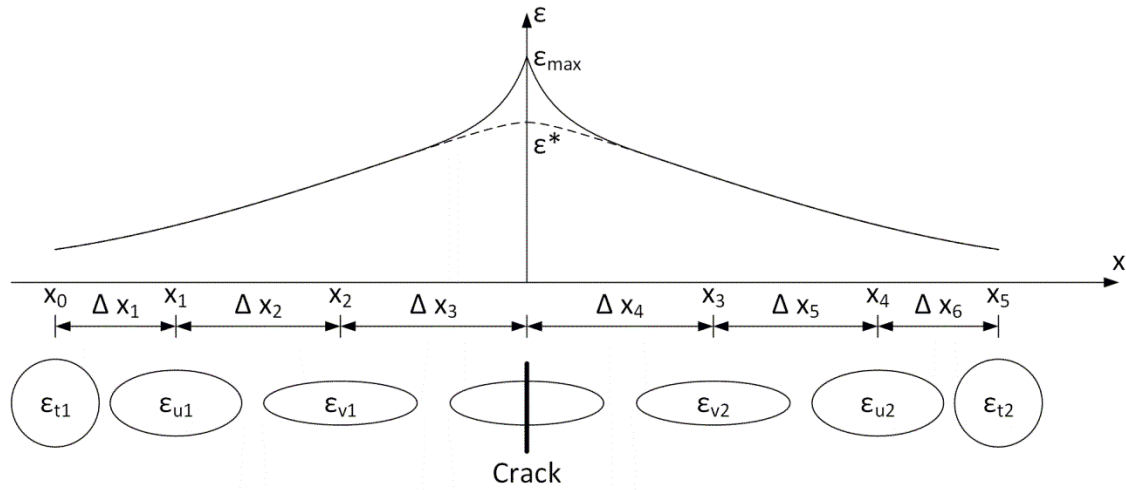
$$\varepsilon_{max} = \ln(2a/d_0) \qquad (1)$$

Figure 2. Interpolation of limit strain ε^*.

where $2a$ is the length of the major axis and d_0 is the diameter of the undeformed circle.

The distribution of ε_{max} is also schematically illustrated in Figure 2. At fracture, ε_{max} goes towards infinity at the crack location. The aim of Veerman's interpolation method is to compute the limit strain ε^* immediately prior to fracture.

To do so, Veerman[8] suggested to use Lagrangian interpolation and listed the formula for the limit strain ε^* as

$$\varepsilon^* = \frac{3}{4}(\varepsilon_{v1} + \varepsilon_{v2}) - \frac{3}{10}(\varepsilon_{u1} + \varepsilon_{u2}) + \frac{1}{20}(\varepsilon_{t1} + \varepsilon_{t2}) \qquad (2)$$

The derivation is, however, not listed in the paper and the mathematical approximations are not mentioned. In the following the derivation is presented.

The basis for Lagrangian interpolation is a polynomial $P_n(x)$,

$$P_n(x) = \sum_{i=0}^{n} L_i(x)\varepsilon(x_i) \qquad (3)$$

where the coefficients $L_i(x)$ are given by

$$L_i(x) = \prod_{\substack{j=0 \\ j \neq i}}^{n} \frac{x - x_j}{x_i - x_j} \qquad (4)$$

and $\varepsilon(x_i)$ is the strain at position x_i. Since six strains are measured, the order of the polynomial is $n = 5$ and as derived in Appendix 1, the coefficients listed in Equation (2) are obtained, when the distance between the centers of the ellipses is assumed to be constant. This is, however, an approximation, which is normally not encountered in practice. Therefore experiments are carried out to determine how well the limit strain is determined with this approximation.

Experiments

Two sets of experiments are conducted; 1) hydraulic bulge tests in a circular and two elliptic dies with two different ratios between major and minor axis of the dies, 2) tensile tests. The 1,0mm thick aluminium AA 1050 blanks are provided with a 2,5mm diameter circle grid with 0,3mm distance between the circles by electro-chemical etching. Loading in bulge tests as well as in tensile tests is performed until fracture occurs. Using a flexible, transparent ruler, the major axis of the ellipses and the distances between the ellipses indicated in Figure 2 are measured in order to calculate the limit strain ε^*. The interpolation is performed using Equation (2) as well as Equation (6) (given in appendix 1).

Materials characterization

1mm thick aluminium 1050 sheets in the "as received" condition are used. Based on the average of two tensile tests, the stress-strain curve is determined as $\sigma_o = 140(\bar{\varepsilon} + 0{,}013)^{0{,}270}$MPa.

Young's modulus $E = 70GPa$ and Poisson's ratio $\nu = 0{,}33$. Isotropic material behaviour is assumed in the FEA.

Bulge tests

Octagonal blanks with a width of 250mm between parallel sides are cut from the aluminium sheet. They are hydraulically bulged to fracture using an in-house build bulge tester (see Figure 3) and three different dies. One die is circular with a diameter of Ø190mm and the two others are elliptical with major/minor axis lengths of 180mm/140mm and 180mm/100mm. The experiments are denoted "circle", "large ellipse" and "small ellipse" respectively in the data treatment. During deformation the blank is clamped by a circular drawbead, which prevents drawing-in of the sheet. During testing the oil pressure is measured. The pressure increase was performed with a manually operated valve, slowly so rate effects should be negligible and the deformation isothermal. The time of a test is typically 2-3 min.

The blanks before and after deformation can be seen in Figure 4.

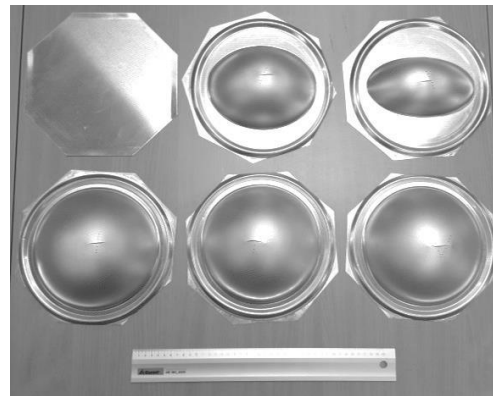**Figure 3.** In-house build bulge tester.

Figure 4. Blanks after bulge tests and an undeformed blank.

Tensile tests

Two tensile tests of strips of dimensions $l_0 \times b_0 = 250 \times 20$ mm provided with

etched circular grid were performed using a 100 kN Amsler universal testing machine (see Figure 5) equipped with a load cell and two length transducers for measuring longitudinal elongation and transversal contraction.

Figure 5. Amsler universal testing machine.

The tensile specimens were clamped by jaws with an original distance of 150mm between them. Elongation and transverse contraction of the sheet width were measured during testing using a longitudinal as well transverse

transducer placed in the mid-section of the sample, where uniaxial deformation prevails. The tensile tests were performed at low speed, app. 0,17 mm/s so rate effects are considered negligible and the deformation isothermal.

The experiments are denoted "tensile testing" in the data treatment.

FEM simulations

Todkar et al.[9] compared experimental bulge test results with numerical simulation using LS-DYNA. Good agreement was found. Therefore LS-DYNA is also utilized in this study.

The numerical simulations are performed using LS-DYNA version R7.1.1. Both bulge tests and tensile tests are modelled with fully integrated shell elements having five through-thickness integration points as utilized in Larsson[10]. The simulation time is 10ms and explicit time integration is used.

Bulge tests

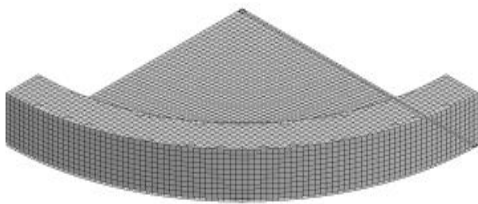A simulation layout of the bulge test with a circular die can be seen in Figure 6.

Figure 6. Bulge test simulation layout. The marked path at the edge is used in the data treatment.

Due to symmetry, only ¼ is modelled. The blank is modelled as circular with a diameter equal to the drawbead diameter and is meshed using 3043 elements. It is clamped along the periphery. The die is modelled as rigid with frictionless contact towards the blank. A pressure increasing linearly with time is assigned to the bottom side of the blank representing the hydraulic oil pressure measured in the experiments. Except for the difference in die geometry, the two

bulge simulations with elliptical dies are performed in the same way.

Examples of the effective plastic strain after bulge testing can be seen in Figure 7-9.
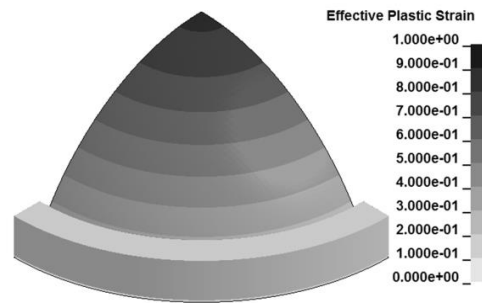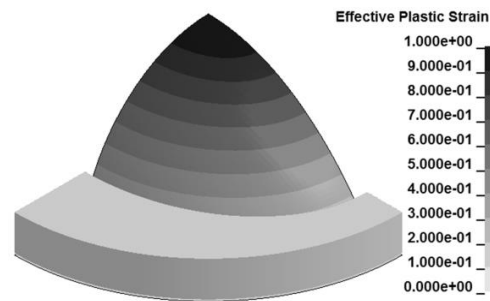

Figure 7. Effective strain, circular die.

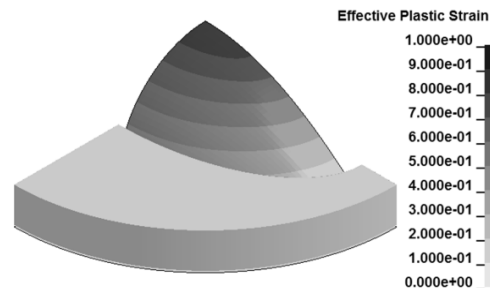**Figure 8.** Effective strain, large ellipse die.

Figure 9. Effective strain, small ellipse die.

Tensile tests

The rectangular aluminium strip is meshed using 3000 elements. Due to the constraining jaws of the tensile test contraction of top and bottom of the specimen is prevented. One end of the specimen is fixed, while the other end moves with constant velocity in longitudinal direction of the strip. The effective plastic strain after onset of necking can be seen in Figure 10.
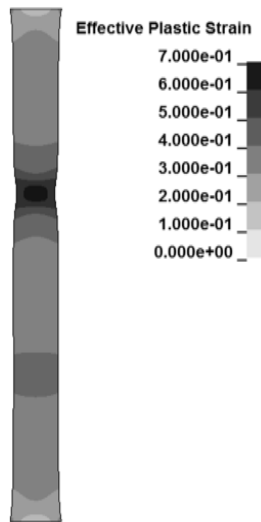

Figure 10. Effective strain after instability has occurred.

For further analysis of the FE-simulations, the effective strain

distribution at instability is plotted along two different paths. For the bulge tests, the effective strain is plotted from the center top of the bulge along the major axis to the periphery of the sheet (see the path in Figure 6) normalized by the instantaneous length from the top to the periphery.

For the tensile test, the path is along the centerline from bottom to top. The resulting effective strain distributions can be seen in Figure 11. The abscissae represents the distance from the bottom normalized with the instantaneous length of the tensile test.
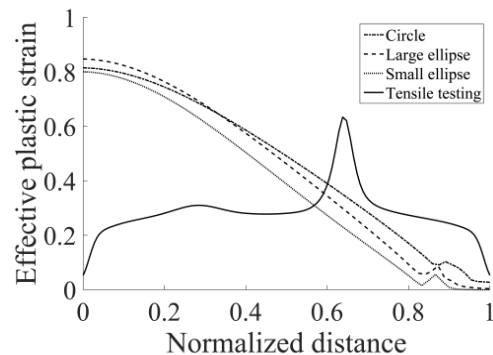

Figure 11. Effective strain along the major axis of bulge tests or centerline of tensile test.

As it can be seen from Figure 11, there is a marked difference in the appearance of the instability strains. For the tensile test, a clear localization of the strain is noticed. For the bulge tests no localization appears. The instability point is here determined by the strain evolution with time. This is described in detail in the following.

Comparison of experiments with FE-simulations

Based on measurements of the deformed grid, the maximum, in-plane limit strain ε^* is calculated using Equations (2) and (6). The minimum in-plane strain is measured directly on the fractured ellipse or the ellipse closest to the fracture. From the FE-simulations, the numerically predicted strain paths and forming limits are extracted from the models.

The resulting experimental strains and numerical strain paths can be seen in Figure 12-13. It should be noticed that since both the pressure and elongation loading are performed with equally sized increments, the rapid increase in strain at the end of loading indicates onset of instability in the FE-simulations. The left most strain path is the one for tensile testing indicating local instability by the abrupt bend towards vertical, i.e. towards plane strain deformation. The three bulge test curves in the stretching region shows no bend, since strain localization is absent. But strain develops faster at the end of the path, where diffuse instability occurs.
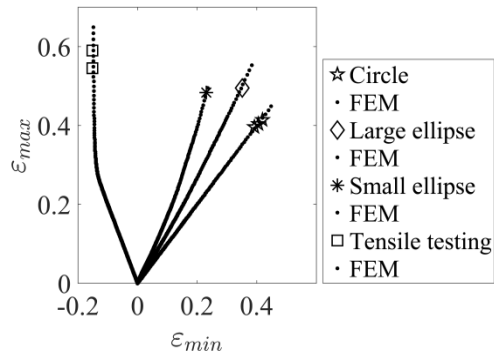
seen in Figure 14. It is noticed that the difference in the two experimental predictions is insignificant.

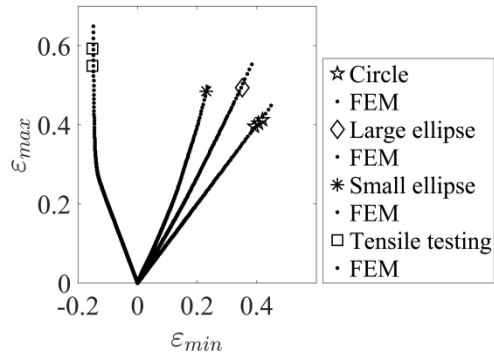**Figure 12.** FE-predicted strain evolution and fracture strains predicted by Veerman's interpolation method.

Figure 13. FE-predicted strain evolution and fracture strains predicted by exact Lagrangian interpolation.
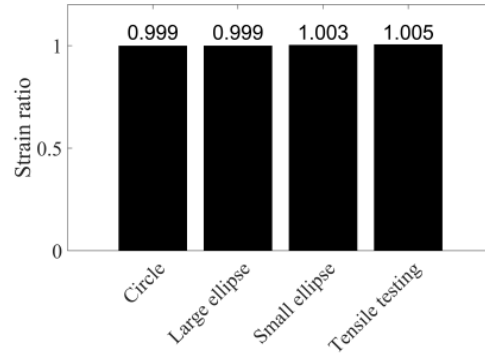
Figure 14. Ratio of maximum in-plane strain determined either by Veerman's interpolation method or exact Lagrangian interpolation. The ratio for each column is indicated above it.

Both Figure 12 and Figure 13 indicate reasonable agreement between prediction of the limit strain by FE-simulations and by experiments.

The ratio of the experimentally determined forming limit based on Veerman's interpolation method and exact Lagrangian interpolation can be

Discussion

The previous section showed that Veerman's interpolation method is in practice just as good as the exact Lagrangian interpolation for the tests investigated.

In order to illustrate whether the assumption of equidistance between centers of ellipses may become insufficient in extreme cases, such a case is analyzed numerically below.

It is assumed that the ellipses denoted t_1 and t_2 in Figure 2 have a maximum in-plane principal strain of 0,1, the ellipses u_1 and u_2 a strain of 0,2 and v_1 and v_2 a strain of 0,3. The spacing between the ellipses is assumed to be $\Delta x_1 = \Delta x_6 = \Delta x$, $\Delta x_2 = \Delta x_5 = (\Delta x)^2$ and $\Delta x_3 = \Delta x_4 = (\Delta x)^3$. This example imitates different levels of violation of the assumption of equidistance between centers of ellipses applied by Veerman[8]. The resulting predicted limit strain ε^*, for various values of Δx, can be seen in Figure 15.

Figure 15 shows that for equally spaced ellipse centers $(\Delta x = 1)$, both Veerman's interpolation formula and the Lagrangian formula are equal as expected. For highly inhomogeneous strain distribution with large difference in distances between ellipse centers, deviations in the calculated limit strain ε^* are obtained. However the difference is fairly small for the selected strains and grid spacing's. Therefore it seems reasonable to apply Veerman's interpolation method instead of the exact Lagrangian interpolation formula.
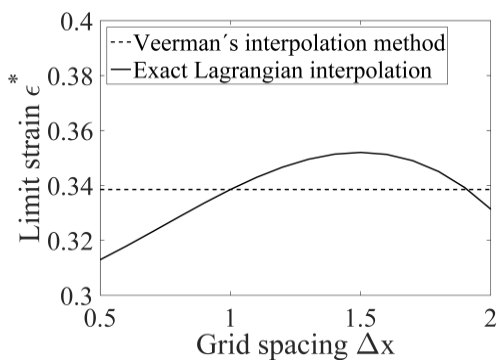

Figure 15. Predicted limit strain for various grid spacing's between ellipse centers when applying Veerman's interpolation method or exact Lagrangian interpolation.

Conclusion

The theoretical basis for Veerman's interpolating method has been established. Experiments of bulge tests with different die sets and tensile tests yielded a variety of different strain paths to fracture. The forming limit strain ε^* were determined from electro-

chemically etched circle grids by using both Veerman's interpolation method and exact Lagrangian interpolation. The experiments were also simulated using FEA.

Based on comparison of experiments with FE-simulations, it can be concluded that for the metal forming processes investigated, bulge testing and tensile testing, Veerman's interpolation method is sufficiently accurate to determine the limit strain ε^*.

Funding

References

1. Keeler J. Determination of forming limits in automotive stampings. *Sheet Met. Ind.* 1965; 42: 683-691.

2. Goodwin GM. Application of strain analysis to sheet metal forming problems in press shop. *La Met. Ital.* 1968; 60-8: 767-774.

3. Takashina K, Herai T, Komorida H and Horita T. Relation Between the Manufacturing Conditions and the Average Strain According to the Scribed Circle Tests in Steel Sheets. *La Met. Ital.* 1968; 60-8: 757-765.

4. Hecker SS. Simple technique for determining limit curves. Sheet Met. Ind. 1975: 671-676.

5. D'Haeyer R., Hecker, A. Determination of the Limiting Strains at the Onset of Necking. *C. R. M.* 1975; 42: 33-35

6. Veerman, CC, Hartman, L, Peels, JJ, Neve, PF. Determination of appearing and admissible strains in cold-reduced sheets. *Sheet Metal Ind.* 1971; 48: 678-680.

7. Volk W. and Hora P. New algorithm for a robust user-independent evaluation of beginning instability for the experimental FLC determination. *Int J Mater Form* 2011; 4: 339–346.

8. Veerman CC. The determination and application of the FLC-onset of localised necking. In: *7th Biennal IDDRG Congress*, Amsterdam, Holland, 1972, pp. 19.1-19.4.

9. Todkar SS, Chhapkhane NK and Todkar SR. Investigation of Forming Limit Curves of Various Sheet Materials Using Hydraulic Bulge Testing With Analytical, Experimental and FEA Techniques. *Int j eng res appl* 2013; 3-1: 858-863.

10. Larsson M. Computational characterization of drawbeads. A basic modeling method for data generation. *J Mater Process Technol* 2009; 209: 376–386.

Appendix 1

Applying Equation (4) to the circle grid seen in Figure 2 yields the following coefficients L_i for $n = 5$

$$L_0 = \left(\frac{x - x_1}{x_0 - x_1}\right)\left(\frac{x - x_2}{x_0 - x_2}\right)\left(\frac{x - x_3}{x_0 - x_3}\right)\left(\frac{x - x_4}{x_0 - x_4}\right)\left(\frac{x - x_5}{x_0 - x_5}\right)$$

$$L_1 = \left(\frac{x - x_0}{x_1 - x_0}\right)\left(\frac{x - x_2}{x_1 - x_2}\right)\left(\frac{x - x_3}{x_1 - x_3}\right)\left(\frac{x - x_4}{x_1 - x_4}\right)\left(\frac{x - x_5}{x_1 - x_5}\right)$$

$$L_2 = \left(\frac{x - x_0}{x_2 - x_0}\right)\left(\frac{x - x_1}{x_2 - x_1}\right)\left(\frac{x - x_3}{x_2 - x_3}\right)\left(\frac{x - x_4}{x_2 - x_4}\right)\left(\frac{x - x_5}{x_2 - x_5}\right)$$

$$L_3 = \left(\frac{x - x_0}{x_3 - x_0}\right)\left(\frac{x - x_1}{x_3 - x_1}\right)\left(\frac{x - x_2}{x_3 - x_2}\right)\left(\frac{x - x_4}{x_3 - x_4}\right)\left(\frac{x - x_5}{x_3 - x_5}\right)$$

$$L_4 = \left(\frac{x - x_0}{x_4 - x_0}\right)\left(\frac{x - x_1}{x_4 - x_1}\right)\left(\frac{x - x_2}{x_4 - x_2}\right)\left(\frac{x - x_3}{x_4 - x_3}\right)\left(\frac{x - x_5}{x_4 - x_5}\right)$$

$$L_5 = \left(\frac{x - x_0}{x_5 - x_0}\right)\left(\frac{x - x_1}{x_5 - x_1}\right)\left(\frac{x - x_2}{x_5 - x_2}\right)\left(\frac{x - x_3}{x_5 - x_3}\right)\left(\frac{x - x_4}{x_5 - x_4}\right)$$

$$(5)$$

By assuming the point of interpolation $x = 0$ and inserting the distances $(\Delta x_1, \Delta x_2, \Delta x_3, \Delta x_4, \Delta x_5, \Delta x_6)$ into Equation (5) gives

$$L_0 = \left(-\frac{\Delta x_2 + \Delta x_3}{\Delta x_1}\right)\left(-\frac{\Delta x_3}{\Delta x_1 + \Delta x_2}\right)\left(\frac{\Delta x_4}{\Delta x_1 + \Delta x_2 + \Delta x_3 + \Delta x_4}\right)\left(\frac{\Delta x_4 + \Delta x_5}{\Delta x_1 + \Delta x_2 + \Delta x_3 + \Delta x_4 + \Delta x_5}\right)\left(\frac{\Delta x_4 + \Delta x_5 + \Delta x_6}{\Delta x_1 + \Delta x_2 + \Delta x_3 + \Delta x_4 + \Delta x_5 + \Delta x_6}\right)$$

$$L_1 = \left(\frac{\Delta x_1 + \Delta x_2 + \Delta x_3}{\Delta x_1}\right)\left(-\frac{\Delta x_3}{\Delta x_2}\right)\left(\frac{\Delta x_4}{\Delta x_2 + \Delta x_3 + \Delta x_4}\right)\left(\frac{\Delta x_4 + \Delta x_5}{\Delta x_2 + \Delta x_3 + \Delta x_4 + \Delta x_5}\right)\left(\frac{\Delta x_4 + \Delta x_5 + \Delta x_6}{\Delta x_2 + \Delta x_3 + \Delta x_4 + \Delta x_5 + \Delta x_6}\right)$$

$$L_2 = \left(\frac{\Delta x_1 + \Delta x_2 + \Delta x_3}{\Delta x_1 + \Delta x_2}\right)\left(\frac{\Delta x_2 + \Delta x_3}{\Delta x_2}\right)\left(\frac{\Delta x_4}{\Delta x_3 + \Delta x_4}\right)\left(\frac{\Delta x_4 + \Delta x_5}{\Delta x_3 + \Delta x_4 + \Delta x_5}\right)\left(\frac{\Delta x_4 + \Delta x_5 + \Delta x_6}{\Delta x_3 + \Delta x_4 + \Delta x_5 + \Delta x_6}\right)$$

$$L_3 = \left(\frac{\Delta x_1 + \Delta x_2 + \Delta x_3}{\Delta x_1 + \Delta x_2 + \Delta x_3 + \Delta x_4}\right)\left(\frac{\Delta x_2 + \Delta x_3}{\Delta x_2 + \Delta x_3 + \Delta x_4}\right)\left(\frac{\Delta x_3}{\Delta x_3 + \Delta x_4}\right)\left(\frac{\Delta x_4 + \Delta x_5}{\Delta x_5}\right)\left(\frac{\Delta x_4 + \Delta x_5 + \Delta x_6}{\Delta x_5 + \Delta x_6}\right)$$

$$L_4 = \left(\frac{\Delta x_1 + \Delta x_2 + \Delta x_3}{\Delta x_1 + \Delta x_2 + \Delta x_3 + \Delta x_4 + \Delta x_5}\right)\left(\frac{\Delta x_2 + \Delta x_3}{\Delta x_2 + \Delta x_3 + \Delta x_4 + \Delta x_5}\right)\left(\frac{\Delta x_3}{\Delta x_3 + \Delta x_4 + \Delta x_5}\right)\left(-\frac{\Delta x_4}{\Delta x_5}\right)\left(\frac{\Delta x_4 + \Delta x_5 + \Delta x_6}{\Delta x_6}\right)$$

$$L_5 = \left(\frac{\Delta x_1 + \Delta x_2 + \Delta x_3}{\Delta x_1 + \Delta x_2 + \Delta x_3 + \Delta x_4 + \Delta x_5 + \Delta x_6}\right)\left(\frac{\Delta x_2 + \Delta x_3}{\Delta x_2 + \Delta x_3 + \Delta x_4 + \Delta x_5 + \Delta x_6}\right)\left(\frac{\Delta x_3}{\Delta x_3 + \Delta x_4 + \Delta x_5 + \Delta x_6}\right)\left(-\frac{\Delta x_4}{\Delta x_5 + \Delta x_6}\right)\left(-\frac{\Delta x_4 + \Delta x_5}{\Delta x_6}\right) \quad (6)$$

If assuming equidistance between the centers of the ellipses ($\Delta x_1 = \Delta x_2 = \Delta x_3 = \Delta x_4 = \Delta x_5 = \Delta x_6 = \Delta x$), Equation (6) reduces to

$$
\begin{aligned}
L_0 &= (-2)\left(-\frac{1}{2}\right)\left(\frac{1}{4}\right)\left(\frac{2}{5}\right)\left(\frac{3}{6}\right) &&= \frac{1}{20} \\[2mm]
L_1 &= (3)(-1)\left(\frac{1}{3}\right)\left(\frac{2}{4}\right)\left(\frac{3}{5}\right) &&= -\frac{3}{10} \\[2mm]
L_2 &= \left(\frac{3}{2}\right)(2)\left(\frac{1}{2}\right)\left(\frac{2}{3}\right)\left(\frac{3}{4}\right) &&= \frac{3}{4} \\[2mm]
L_3 &= \left(\frac{3}{4}\right)\left(\frac{2}{3}\right)\left(\frac{1}{2}\right)(2)\left(\frac{3}{2}\right) &&= \frac{3}{4} \\[2mm]
L_4 &= \left(\frac{3}{5}\right)\left(\frac{2}{4}\right)\left(\frac{1}{3}\right)(-1)(3) &&= -\frac{3}{10} \\[2mm]
L_5 &= \left(\frac{3}{6}\right)\left(\frac{2}{5}\right)\left(\frac{1}{4}\right)\left(-\frac{1}{2}\right)(-2) &&= \frac{1}{20}
\end{aligned}
\tag{7}
$$